CHEMISTRY OF MATERIALS

Article

pubs.acs.org/cm

Effect of Seed Age on Gold Nanorod Formation: A Microfluidic, Real-Time Investigation

John Watt, Bradley G. Hance, Rachel S. Anderson, and Dale L. Huber*

Sandia National Laboratories, Albuquerque, New Mexico 87105, United States

Supporting Information

ABSTRACT: We report a real time investigation into the effect of seed age on the growth of gold nanorods using a microfluidic reaction apparatus. Through small-angle X-ray scattering (SAXS) and ultraviolet−visible spectroscopy (UV−vis) analysis, we observe the seeds aging in accordance with Ostwald ripening. A seed solution is then aged in situ and continuously injected into a microfluidic chip to initiate rod growth. We track nanorod formation in real time using in-line ultraviolet−visible and near-infrared (UV−vis−NIR) monitoring and observe a dramatic decrease in yield with increasing seed age. We then demonstrate that, by diluting the gold seed solution immediately following synthesis, the rate of aging can be reduced and nanorods synthesized continuously, in good yield. These findings suggest ultrasmall, catalytically active seeds, which are rapidly lost due to ripening and are critical for the formation of gold nanorods.

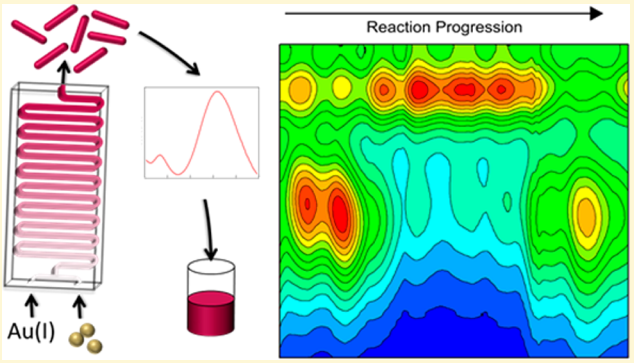

Gold nanorods have attracted significant research interest in the past decade due to their multiple plasmon absorption bands, the transverse and longitudinal surface plasmon resonances (LSPRs). The LSPR is highly sensitive to the rod aspect ratio, allowing it to be tuned across a broad wavelength range.[1,2] This has seen gold nanorods utilized in a number of applications including chemical sensing, bioimaging, theranostics, and surface enhanced spectroscopy.[3−6] Absorption and scattering phenomena become dominant at different aspect ratios, and gold nanorods can be targeted to photothermal or optical applications depending on their dimensions. Therefore, robust understanding and good synthetic control over nanorod growth is essential for effective material application. The growth of gold nanorods has been reported by electrochemical methods via the use of hard templates, seedless one-step growth, and multistep growth mechanisms.[6−10] However, it is the silver assisted, seeded growth mechanism using the quaternary ammonium surfactant, cetyltrimethylammonium bromide (CTAB), which has received the most attention.[11−18] Here, small preformed gold nanoparticles are used as seeds for the further addition of gold monomer, resulting in anisotropic growth. This facile wet-chemical method is versatile and scalable and allows for a wide range of gold nanorod sizes to be synthesized.[19,20]

There are a number of studies which have given valuable information on the effect of varying reaction parameters on gold nanorod formation, including reagent and seed concentrations, pH, and the addition of organic additives.[10,21−28] The effect of variation in size and structure of the gold seed nanoparticles, however, is less well established. Since the gold seed nanoparticles act as templates for anisotropic growth their structure has a direct effect on the formation of the gold nanorods. For example, gold nanorods with observable lamellae defects have been shown to grow from multiply twinned nanoparticle seeds.[29−31] Gold seed nanoparticles, however, possess a small size and large free surface energy and are subject to changes in size and size distribution via aging; therefore, their age should also have a direct influence on nanorod formation. The reported ages of seed nanoparticles used for gold nanorod formation varies significantly, from 5 min to up to one month.[32−35] A few studies have suggested an optimal aging time for their systems; however, this is not commonplace.[22,23] Therefore, a comprehensive investigation into the effect of seed age on gold nanorod formation is still required. Investigation by multiple batch syntheses has been reported, but uncontrollable aging can occur during aliquot removal and preparation for ex situ investigation, leading to uncertainty.[32,36−38] Furthermore, aliquot removal is time-consuming and can lead to incomplete data due to gaps in the time series.

Recently, microfluidic-based devices have been effectively employed to investigate a variety of different reactions in organic synthesis, heterogeneous catalysis, and inorganic nanoparticle synthesis.[9,39−43] Reducing the reaction volume to the microliter scale allows for rapid and reproducible variation of external reaction parameters such as temperature and concentration. Furthermore, the approach is well suited to in-line monitoring by optical techniques, e.g., UV−vis−NIR

Received: July 13, 2015
Revised: September 1, 2015
Published: September 2, 2015

DOI: 10.1021/acs.chemmater.5b02675
Chem. Mater. 2015, 27, 6442−6449

spectroscopy. As such, microfluidic devices allow for the real time effect of a change in a reaction parameter to be observed and, hence, the optimization of reaction kinetics and product yield.

Here we use a continuous flow microfluidic device to investigate the effect of seed age on the growth of gold nanorods in real time. The gold nanorods were synthesized following the popular Nikoobakht method with modifications applied for a microfluidic setup.[44] Gold nanorod formation was monitored in-line with UV−vis−NIR spectroscopy. To give real time information on the effect of seed age on the growth of gold nanorods a seed solution was freshly prepared and then continuously injected onto a microfluidic chip where it was mixed with a growth solution to initiate rod formation. We then observe the formation of gold nanorods as a direct dependence on seed age.

EXPERIMENTAL SECTION

Materials. Gold(III) chloride hydrate (~52% Au) and hexadecyltrimethylammonium bromide (≥99%, Lot no. SLBD0174 V) were purchased from Sigma-Aldrich. $AgNO_3$ (ACS) and HCl (ACS) were purchased from Fisher Scientific. Ethanol (ACS/USP) was purchased from Pharmco-Aaper. $NaBH_4$ (99%) was purchased from Acros. *N*-Octyldiisopropylchlorosilane was purchased from Gelest.

Solution Preparation. The growth solution, ascorbic acid solution, CTAB solution, and seed solution were prepared as follows. For the growth solution; 1 mL of 10 mM $HAuCl_4$ solution was added to 8.8 mL of 0.05 M CTAB solution stirring (550 rpm) at 30 °C, followed by 0.1 mL of conc HCl (12.1 N) and 50 μL of a 40 mM $AgNO_3$ solution. For the ascorbic acid solution, 37.2 mg of ascorbic acid was dissolved in 100 mL of DI water to give a concentration of 2.1 mM. For the seed solution used in the in situ aging experiment, SAXS analysis, and UV−vis−NIR analysis, 0.25 mL of 10 mM $HAuCl_4$ solution was added to 9.75 mL of 0.1 M CTAB solution stirring rapidly (1200 rpm) at 30 °C. Then a 1 mmol solution of $NaBH_4$ was prepared in ice cold water. 60 μL of this was diluted to 600 μL with ice cold water and injected rapidly to the gold−CTAB solution inducing a color change from pale yellow to brown-yellow. This was stirred at 1200 rpm for 1 min before being diluted 1 in 4 with 0.05 M CTAB. This solution was also used for ex situ SAXS and UV−vis aging experiments. The seed solution used for the predilution experiment was prepared in the same manner; however, the final dilution factor was 1 in 28.

Cell Silanization. The microfluidic cell (Dolomite 1000 μL Glass Microreactor Chip 3 Input, Part no. 2100146) was first cleaned with aqua regia (1:3 HNO_3:HCl), followed by rinsing with DI water and ethanol. It was then flushed with dry N_2 and dried overnight under vacuum at 150 °C. The cell was then cooled to room temperature in a drybox. A 5% solution of *n*-octyldiisopropylchlorosilane in toluene was injected into the cell. The cell was plugged and sealed and placed in an incubator at 70 °C for 40 h. Following this the cell was rinsed with toluene and placed under vacuum at 150 °C. The cell was then cooled to room temperature and primed with DI water before the injection of the reaction solutions.

On-Chip Gold Nanorod Synthesis. In a typical experiment, the microfluidic cell was placed on a Peltier heater set to 25 °C. For the in situ aging experiment, the growth solution containing Au(III) was injected via an Asia Module Syringe Pump into a PEEK mixing tee where it was mixed with the ascorbic acid solution (injected via a Chemyx Fusion200 Syringe Pump), thereby reducing Au(III) to Au(I). Observation of the fluid lines post mixing tee showed a yellow to colorless color change, indicating complete reduction of Au(III). The seed solution was injected via a Chemyx Fusion200 Syringe Pump and diluted in-line via a PEEK mixing tee with a 0.05 M CTAB solution (injected via an Asia Module Syringe Pump). The Au(I) solution and diluted seed solution were then mixed together on-chip in the mixing channel to initiate rod growth. The growth, seed, and dilute solutions were kept at 30 °C; the ascorbic acid solution was kept at room temperature. Flow rates were set to 5 μL min^{-1}, 3.6 μL min^{-1}, 1 μL min^{-1}, and 6 μL min^{-1} for the growth, ascorbic acid, seed, and dilute CTAB solutions, respectively. These flow rates combine to give a residence time-on-chip of 70 min, after accounting for additional tubing length. The as-synthesized gold nanorods were characterized in-line using a flow through optical fiber UV−vis−NIR spectrometer (Ocean Optics, USB2000). For the predilution experiments, the growth and ascorbic acid solutions were set up identical to above. The seed solution, however, was diluted with a 0.05 M CTAB solution at t = 1, 10, or 25 min after synthesis ex situ, kept at 30 °C, and injected directly onto the chip at 7 μL min^{-1}.

Characterization. Small angle X-ray scattering (SAXS) experiments were carried out by removing a 7.5 mL aliquot from the aging seed solution and freezing in liquid nitrogen to halt aging. These were then dried on a freeze drier (Labconco, Freezone 2.5) before adding 300 μL of DI water to yield a concentrated solution of gold seed nanoparticles suitable for analysis. 80 μL of the sample was loaded into a 1.0 mm diameter borosilicate glass capillary (Charles Supper Company, Natick, MA) and analyzed using a Rigaku Smartlab diffractometer system with Smartlab Guidance system control software. Cu Kα radiation (40 kV, 44 mA) was used in transmission geometry with a scintillation detector. Data analysis was performed using Rigaku NANO-Solver v.3.5 software, assuming a spherical particle shape and log-normal size distribution. Ex situ UV−vis spectroscopy was performed using a Cary 6000i UV−vis−NIR spectrometer with a Varian Dual Cell Peltier circulation heater set to 30 °C. Absorbance profiles were collected from 300 to 800 nm every 2 min. Data was analyzed using Origin Pro v9.1. High resolution transmission electron microscopy (HRTEM) analysis of gold nanorods was performed by freezing out excess CTAB at 4 °C and centrifugation. The resulting solution was then diluted in DI water and dropcast onto a carbon coated copper grid (SPI, Westchester, PA). Images were collected using a Philips Tecnai HRTEM operating at 300 keV.

RESULTS

To properly understand this effect, analysis of the gold seed nanoparticles under experimental aging conditions is first required. Therefore, a solution of gold seed nanoparticles was prepared and aged at 30 °C (to maintain solubility of the CTAB surfactant) for 300 min and characterized using small-angle X-ray scattering (SAXS) and UV−vis spectroscopy. A typical SAXS experiment including the model fit and residual errors are shown in Figure 1a. SAXS data was fitted assuming a spherical form factor and log-normal distribution (for full SAXS analysis, see Supporting Information, Figure S1).[38] Figure 1b gives the SAXS calculated diameter and coefficient of variation of a number of aliquots taken from the aging seed solution. Each aliquot was quenched by freezing in liquid nitrogen to halt aging, followed by freeze-drying and suspension in a small volume of water for SAXS analysis. From t_{seed} = 0 to t_{seed} = 60 min we observe a sharp increase in the average seed size from 2.1 to 2.4 nm. This is followed by a slight increase to 2.6 nm at t_{seed} = 180 min which is then maintained to t_{seed} = 300 min. The coefficient of variation of the nanoparticle seeds decreases from 58% to 33% over the course of aging indicating a tightening of the size distribution with increased nanoparticle size. Attempts to confirm SAXS size analysis with transmission electron microscopy (TEM) were unsuccessful due to uncontrollable aging, or "reaction creep", observed during aliquot removal and sample preparation.[38] The use of alkanethiol phase transfer agents and product isolation via addition of a nonsolvent (i.e., EtOH or MeOH) and centrifugation was observed to rapidly increase the aging rate, leading to large discrepancies between size analyses. In contrast, reaction creep in SAXS analysis was

DOI: 10.1021/acs.chemmater.5b02675
Chem. Mater. 2015, 27, 6442−6449

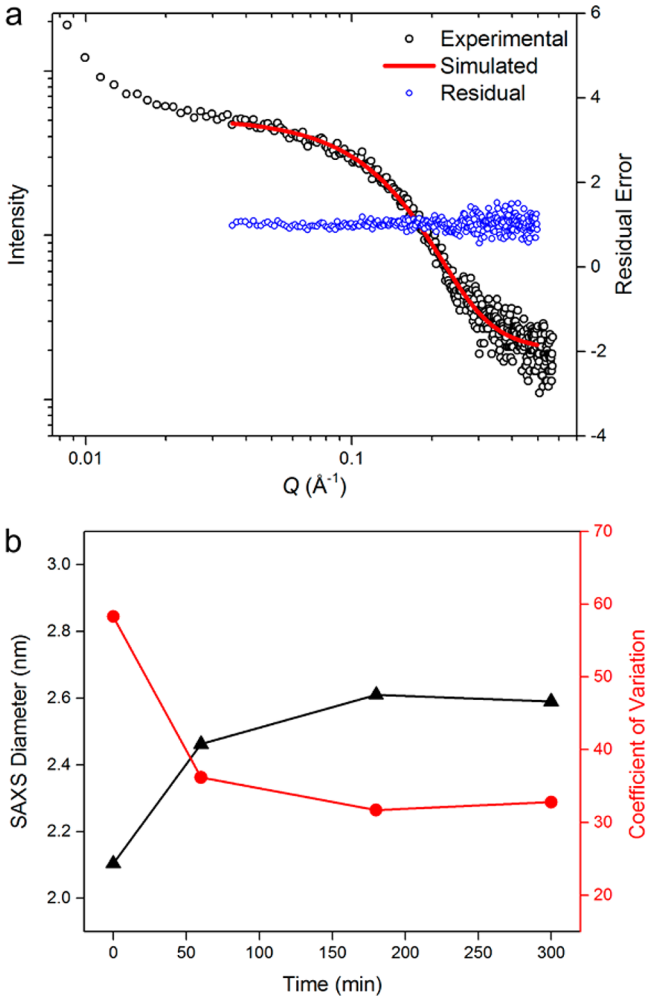

Figure 1. Small angle X-ray scattering (SAXS) experiments of aliquots taken from an aging gold seed nanoparticle solution. (a) A typical experiment showing the raw data, model fit, and residual errors. (b) A plot of SAXS calculated mean diameter (black) and coefficient of variation against aging time (red).

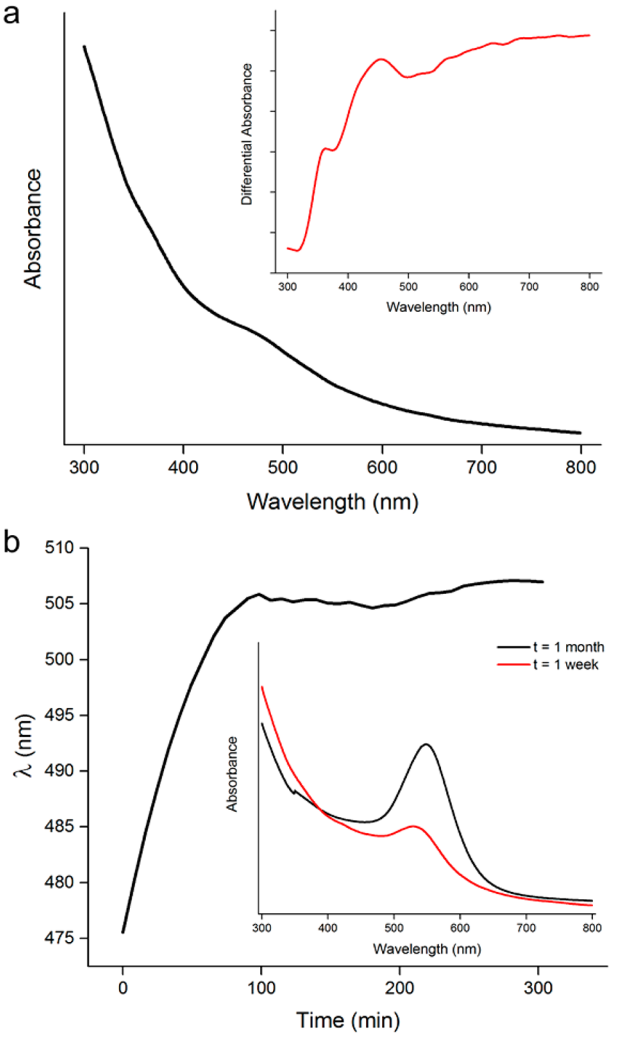

Figure 2. UV−vis spectroscopy analysis of a solution of gold seed nanoparticles aging at 30 °C. (a) The UV−vis absorbance profile of the seed solution at t_{seed} = 0, with the differential absorbance (first derivative of absorbance) given in the inset. (b) Wavelength of the first absorbance peak of the gold seed nanoparticles plotted against aging time and (inset) the absorbance profile of the seed solution aged for 1 week (red line) and 1 month (black line).

controlled by immediately quenching the solution and measuring at low temperature.

For UV−vis analysis a solution of gold seed nanoparticles was aged in situ at 30 °C for 300 min to give real time data, as shown in Figure 2 (complete UV−vis spectra are given in Figure S2). Figure 2a shows the absorbance profile at t_{seed} = 0 along with a plot of the differential absorbance (see inset). We observe a first absorption peak at 475 nm, with a secondary absorption at 369 nm. We then track the evolution of the first absorption peak over the course of the aging experiment (Figure 2b). Here we observe an increase from 475 to 505 nm over 90 min. The absorption peak increases slightly through the remainder of the experiment to 507 nm at t_{seed} = 300 min. The seed solution was then kept at 30 °C for one month, and an increase in intensity of the SPR signal and redshift to >520 nm was observed (see inset, Figure 2b). This observation indicates a transition from molecular like optical transitions to the emergence of a surface plasmon resonance (SPR). In Figure 2a the spectrum is dominated by a broad absorption stretching into the UV which is characteristic of gold nanoparticles less than 2 nm in size. The absorption features visible at 475 and 369 nm can be attributed to intraband (sp → sp) and interband (d → sp) molecular-like transitions that arise when nanoparticles decrease to below 1.6 nm in size.[38,45−47] As the gold seed solution ages, we see a red-shift of the absorption to a wavelength typical of a SPR. This surface plasmon absorption is characteristic of nanoparticles with a diameter of 2 nm or larger.[46]

Therefore, from both SAXS experiments and UV−vis spectroscopy we can be certain that there is a significant population of gold seed nanoparticles less than 2 nm in size at t_{seed} = 0. This has been observed previously for gold seed solutions prepared by a similar method.[32,33] As the seed solution ages, there is an increase in the average nanoparticle diameter and a decrease in the size dispersity. This indicates the dissolution of small, high energy, and high curvature nanoparticles as expected for Ostwald ripening.[48−52]

In order to investigate the effect that this observation has on gold nanorod formation we employed a continuous flow microfluidic device and performed a typical seed mediated gold nanorod synthesis on-chip (Scheme 1). Here, an Au(III) precursor is reduced in-line by a weak reducing agent, ascorbic acid, yielding Au(I). A gold seed nanoparticle solution is kept at

DOI: 10.1021/acs.chemmater.5b02675
Chem. Mater. 2015, 27, 6442−6449

Scheme 1. Schematic Illustration of the Microfluidic Apparatus Used To Investigate the Formation of Gold Nanorods in Real Time

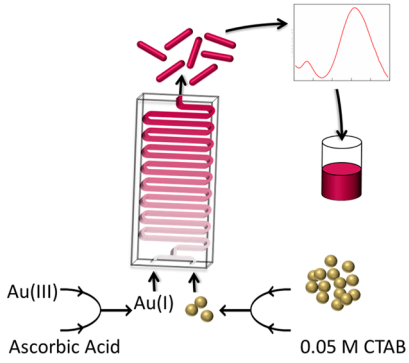

30 °C to replicate aging conditions and is diluted in-line by a CTAB solution. The Au(I) and dilute seed solutions are then simultaneously introduced into the microfluidic chip, and growth is initiated in a mixing channel. Flow rates were adjusted to ensure an appropriate seed:Au(I) ratio for good nanorod yield. Nanorod growth was visually observed by the appearance of a color gradient in the reaction channel (Figure S3). It should be noted that both the mixing channel and the reaction channel have Reynolds numbers < 1, indicating purely laminar flow. The reaction product is characterized in situ by an in-line UV−vis−NIR detector and then collected for ex situ characterization. Ex situ characterization of a typical reaction product is given in Supporting Information, Figures S4 and S5. The as-synthesized gold nanorods are single crystalline with no visible defects or twin planes. Microfluidic channel fouling is mitigated by pretreatment of the glass cell with a hydrophobic silane coating. This reduces particle interaction at the channel interface and enables blockage free operation for several hours, which is comparable to droplet based systems.[41,42,53]

Figure 3 shows the effect of an aging seed solution on gold nanorod formation, in real time. A 2D UV−vis−NIR contour plot is shown in Figure 3a with a transverse SPR located at λ_{max} = 525 nm and a longitudinal SPR at λ_{max} = 735 nm, indicating the formation of gold nanorods. The periodic pulsing behavior can be attributed to the flow profile of the pump. To account for this and to give a means to easily track the yield of gold nanorods, the relative peak area (A_L/A_T) is calculated and plotted against reaction time (Figure 3b). Since the seed solution is used immediately, reaction time also corresponds directly to seed age. Here, the trace begins at t = 70 min, which, due to the residence time of the chip, corresponds to the emergence of nanorods synthesized when seed age t_{seed} = 0. Note that the nanorod yield is already greater than one due to forward diffusion in the microfluidic channels. We then observe four stages in the reaction. Stage I is the time period taken for the reaction to reach a steady state in reagent concentration. This occurs due to the parabolic flow profile inherent in microfluidic channels, which can be modeled using Poiseuille's Law for laminar flow (for full analysis, see Supporting Information). Here we predict a time to steady state concentration of 85.0 min after the first observation of nanorod formation, which matches closely to what is observed in Figure 3b. In stage II we observe a maximum nanorod yield. Then, there is a decline in the longitudinal plasmon resonance and an increase in the transverse response (see Figure 3a). This corresponds to an increase in the formation of spheres at the

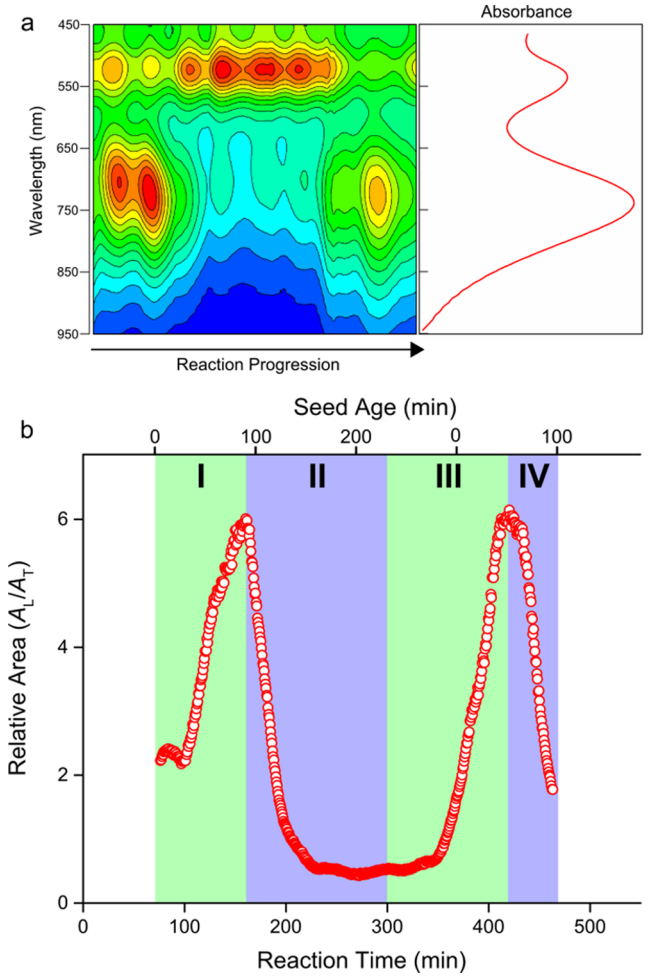

Figure 3. Real time UV−vis−NIR analysis of gold nanorods formed from an aging gold seed solution. (a) 2D contour plot of the UV−vis−NIR analysis plotted against reaction progression, along with a single UV−vis trace oriented to match the position of peaks in the real-time trace. (b) Plot of relative peak area (A_L/A_T) against reaction time with four reaction stages; (I) emergence of nanorods and developing of a steady state reaction, (II) decrease in nanorod yield following a maximum yield, (III) injection of fresh seed solution at 300 min, and (IV) decrease in nanorod yield from a second maximum.

expense of rods, leading to a rapid drop in A_L/A_T. Rod yield then remains constant for ∼100 min. At 300 min (stage III) we inject a freshly prepared gold seed solution onto the microfluidic chip. We then observe an increase in A_L/A_T and the second emergence of a steady state seed concentration, similar to stage I. Finally, there is stage IV, where nanorod yield rapidly declines, behavior which is similar to stage II.

Therefore, from Figure 3 it can be observed that as the solution of gold seed nanoparticles ages, the nanorod yield decreases. This has previously been observed in batch investigation, albeit over a much longer time scale, by Jiang and Pileni.[32] To confirm our observation a number of ex situ batch reactions were performed (Figure S6). Also, experiments injecting fresh growth and ascorbic acid solutions resulted in a continued decrease in nanorod yield, further supporting the influence of the seed nanoparticles (Figure S7). From the above results, it was hypothesized that a fresh seed solution is critical for nanorod formation.

To test this we diluted the seed nanoparticles with a CTAB solution immediately following synthesis. The dilution of a

DOI: 10.1021/acs.chemmater.5b02675
Chem. Mater. 2015, 27, 6442−6449

nanoparticle solution should dramatically decrease the rate of Ostwald ripening due to a decrease in both the dissolution and redeposition rates of gold atoms.[54−57] The diluted seed solution was then injected directly onto the chip and mixed with Au(I) to initiate rod growth. Flow rates were adjusted to ensure that the residence time and overall seed:Au(I) ratio remained consistent with the previous experiment.

Figure 4a shows the 2D UV−vis−NIR contour plot made with a seed solution diluted at t_{seed} = 1 min. The corresponding

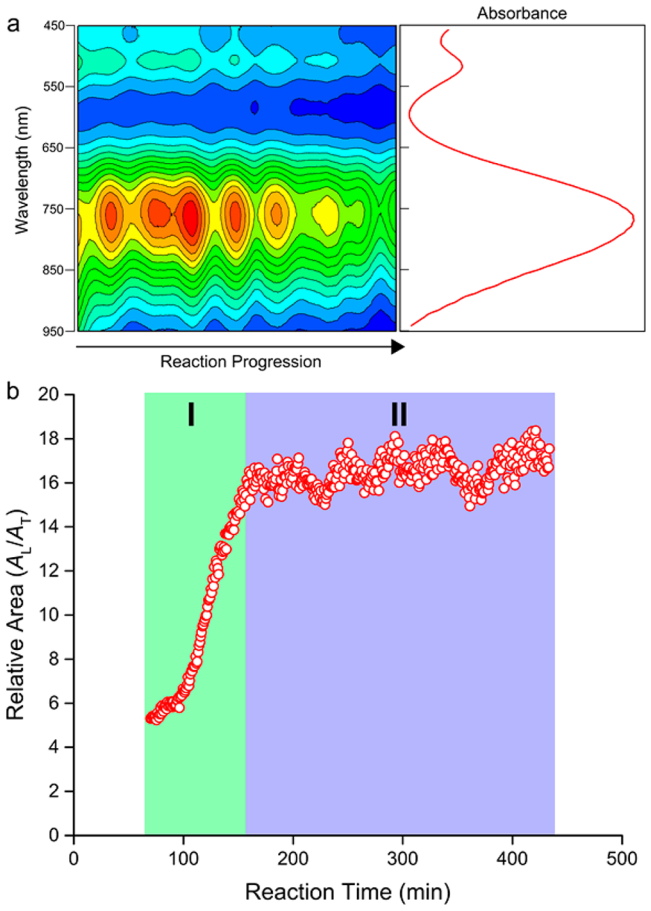

Figure 4. Real time UV−vis−NIR analysis of gold nanorods formed from a prediluted gold seed solution. (a) 2D contour plot of the UV−vis−NIR analysis plotted against reaction progression, along with a single UV−vis trace oriented to match the position of peaks in the real-time trace. (b) Plot of relative peak area (A_L/A_T) against reaction time with two reaction stages; (I) emergence of nanorods and developing of a steady state reaction and (II) continued growth of nanorods in high yield.

relative peak area (A_L/A_T) trace (Figure 4) shows a nanorod yield almost three times greater than that observed in the in situ aging experiment (see also Supporting Information). Furthermore, this high yield is maintained for over 4 h of reaction time. The reaction carried out with a diluted seed solution can then be understood in two stages: (I) the emergence of a steady state and (II) continued growth of gold nanorods in high yield.

Additional predilution experiments were then carried out, with dilutions made at t_{seed} = 1, 10, and 25 min. The relative area of each experiment calculated in the steady state growth stage is plotted against reaction time (Figure 5a) along with standard deviation between repeat experiments (inset). Here we observe a number of important features. First, the standard deviation between experiments decreases with seed age. This can be attributed to the timing error inherent in the manual dilution step. Despite efforts to time this step exactly for each experiment, the rapid rate of seed aging in the early stages introduces significant uncertainty. As the aging progresses, its rate decreases and the manual timing error becomes less important. Second, the nanorod yield decreases rapidly with increasing dilution time. This corresponds to an increasing seed age which matches with our observation in the in situ aging experiment (Figure 3). This data can be fit with a power law to give a $t^{(-0.71)}$ dependency of nanorod yield on seed age. Ostwald ripening theory predicts an increase in average nanoparticle size that follows $\bar{R} \propto t^{(0.33)}$.[58] Therefore, ripening of the entire ensemble could not be used to explain the rapid decrease in nanorod yield (which would then have a $t^{(-0.33)}$ dependency). To understand how the aging seed population is changing and how this could influence nanorod yield we plotted the size distribution profiles taken from SAXS analysis, shown in Figure 5b. Then by integrating from $0 < d < x$ nm, for different values of x, we can investigate how different populations of gold seed nanoparticles are aging with time (see Supporting Information, Figure S8). Here, we found that the population of seed nanoparticles $0 < d < 1.1$ nm in size decreases with a $t^{(-0.70)}$ dependency (Figure 5c), similar to that observed for nanorod yield.

DISCUSSION

These results suggest that for our system a fresh seed solution with a population of ultrasmall gold seed nanoparticles is critical for the formation of gold nanorods in high yield. A similar effect has previously been observed by Jana, who showed that seed nanoparticles larger than 3.5 nm led to a very low yield of gold nanorods.[20] These observations were explained by a soft template mechanism, wherein the larger nanoparticle seeds could not interact with the cylindrical CTAB micelles and hence their growth could not be directed anisotropically. Here, however, we observe a critical size of around 1 nm, which cannot be explained by the soft template mechanism. Other mechanisms to explain the anisotropic growth of gold nanorods include the formation of a CTA−Br−Ag^+ complex which acts as a selective capping agent on the lateral sides of the nanorod, under-potential deposition of a monolayer of silver metal, the formation of ion channels in the CTAB bilayer, and a prevailing electric field leading to selective deposition of Au(I) at the nanorod tips.[1,15,35,59] A simpler, more widely accepted idea is that the increased curvature of the CTAB bilayer at the gold nanorod tips allows for increased access by gold monomer.[1] While valuable, these explanations cannot be applied to the very early stages of gold nanorod formation as they assume some structural anisotropy is already present. The emergence of anisotropy from the gold seed nanoparticles has been explained by the presence of crystal defects or through the selective addition of gold monomer to well-defined crystal facets.[15,29−31] However, as has been made evident here and in other studies, ex situ characterization of gold seed nanoparticles can introduce significant uncertainty through nanoparticle aging during sample preparation.[38] Furthermore, gold nanoparticles can possess a number of different structural motifs at low sizes, and structural transitions can occur.[60−63] Therefore, it can be difficult to identify the exact nature of the seed responsible for anisotropic growth, especially in a seed solution with a mixture of nanoparticle structures.

DOI: 10.1021/acs.chemmater.5b02675
Chem. Mater. 2015, 27, 6442−6449

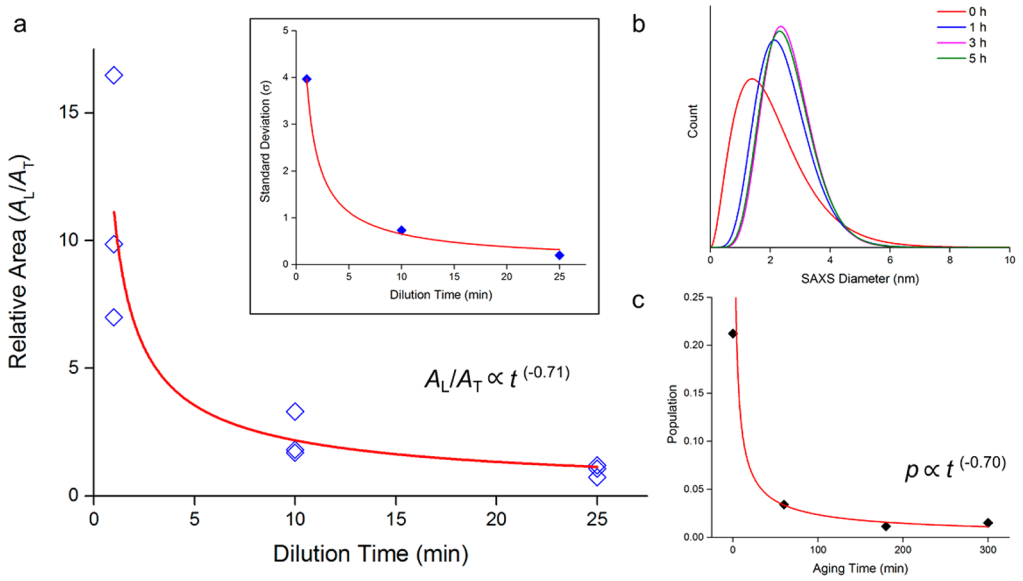

Figure 5. Predilution experiments. (a) Plot of relative peak area (A_L/A_T) against dilution time, with standard deviation of repeat experiments (inset). (b) Size distribution profiles for an aging seed nanoparticle solution, taken from SAXS analysis. (c) Population of seed nanoparticles $0 < d < 1.1$ nm in size, as a function of time.

The current results suggest that ultrasmall gold seed nanoparticles are responsible for high yield nanorod growth. This corresponds to high curvature, high surface energy gold nanoparticles which are characterized by incomplete coverage of the CTAB bilayer and low coordination surface sites. Gold nanoparticles below 2 nm in size have shown superior catalytic behavior when supported on inert substrates, with similar catalytic promise displayed when unsupported.[64−66] Recently, Hubert et al. recently showed that the reduction of Au(I) to Au(0) only occurs at the surface of the gold nanorod.[12] This would suggest that the catalyzed reduction of Au(I) at the surface of the gold nanoparticle seeds leads to the emergence of anisotropy. As the nanoparticles ripen there is a loss of curvature and an improvement in CTAB bilayer coverage, thus reducing their ability to catalytically reduce Au(I).

CONCLUSION

In summary, we have used a microfluidic reaction setup to show that a freshly prepared gold nanoparticle seed solution is critical for the formation of gold nanorods in high yield. This is due to the presence of ultrasmall, high energy, catalytically active gold seed nanoparticles that are responsible for the emergence of anisotropy. As the seed nanoparticle solution ages the average seed size increases and the nanorod yield decreases. By diluting the seed solution immediately following synthesis, the rate of aging can be made negligible and gold nanorods formed constantly, in high yield. Full structural analysis of the ultrasmall nanoparticles responsible for the emergence of anisotropic growth is a subject of further investigation. However, the current study suggests that preparation for ex situ investigation can introduce uncertainty through uncontrolled aging, and great care must be taken to ensure that artifacts are not introduced into the analysis. By diluting the seed nanoparticles immediately following synthesis, aging can be halted, which will provide a means to probe their structure closer to their natural state.

ASSOCIATED CONTENT

Supporting Information

The Supporting Information is available free of charge on the ACS Publications website at DOI: 10.1021/acs.chemmater.5b02675.

Complete SAXS analysis, ex-situ characterization, and further experiments (PDF)

AUTHOR INFORMATION

Corresponding Author

*(D.L.H.) E-mail: dale.huber@sandia.gov.

Author Contributions

The manuscript was written through contributions of all authors. All authors have given approval to the final version of the manuscript.

Notes

The authors declare no competing financial interest.

ACKNOWLEDGMENTS

This research was supported by the U.S. Department of Energy, Office of Basic Energy Sciences, Division of Materials Science and Engineering. Microfluidic reactions, HRTEM imaging, and SAXS measurements were performed at the Center for Integrated Nanotechnologies, a U.S. Department of Energy, Office of Basic Energy Sciences, user facility. Sandia National Laboratories is a multiprogram laboratory managed and operated by Sandia Corporation, a wholly owned subsidiary of Lockheed Martin Corporation, for the U.S. Department of Energy's National Nuclear Security Administration under Contract DE-AC04-94AL85000.

REFERENCES

(1) Lohse, S. E.; Murphy, C. J. The Quest for Shape Control: A History of Gold Nanorod Synthesis. *Chem. Mater.* **2013**, *25*, 1250−1261.

(2) Alekseeva, A. V.; Bogatyrev, V. A.; Khlebtsov, B. N.; Mel'nikov, A. G.; Dykman, L. A.; Khlebtsov, N. G. Gold nanorods: Synthesis and optical properties. *Colloid J.* **2006**, *68*, 661−678.

DOI: 10.1021/acs.chemmater.5b02675
Chem. Mater. 2015, 27, 6442−6449

(3) Vigderman, L.; Khanal, B. P.; Zubarev, E. R. Functional Gold Nanorods: Synthesis, Self-Assembly, and Sensing Applications. *Adv. Mater.* **2012**, *24*, 4811−4841.
(4) Nepal, D.; Park, K.; Vaia, R. A. High-Yield Assembly of Soluble and Stable Gold Nanorod Pairs for High-Temperature Plasmonics. *Small* **2012**, *8*, 1013−1020.
(5) Huang, X.; Neretina, S.; El-Sayed, M. A. Gold Nanorods: From Synthesis and Properties to Biological and Biomedical Applications. *Adv. Mater.* **2009**, *21*, 4880−4910.
(6) Perez-Juste, J.; Pastoriza-Santos, I.; Liz-Marzan, L. M.; Mulvaney, P. Gold nanorods: Synthesis, characterization and applications. *Coord. Chem. Rev.* **2005**, *249*, 1870−1901.
(7) Jana, N. R.; Gearheart, L.; Murphy, C. J. Wet chemical synthesis of high aspect ratio cylindrical gold nanorods. *J. Phys. Chem. B* **2001**, *105*, 4065−4067.
(8) Jana, N. R.; Gearheart, L.; Murphy, C. J. Seed-mediated growth approach for shape-controlled synthesis of spheroidal and rod-like gold nanoparticles using a surfactant template. *Adv. Mater.* **2001**, *13*, 1389−1393.
(9) Bullen, C.; Latter, M. J.; D'Alonzo, N. J.; Willis, G. J.; Raston, C. L. A seedless approach to continuous flow synthesis of gold nanorods. *Chem. Commun.* **2011**, *47*, 4123−4125.
(10) Ali, M. R. K.; Snyder, B.; El-Sayed, M. A. Synthesis and Optical Properties of Small Au Nanorods Using a Seedless Growth Technique. *Langmuir* **2012**, *28*, 9807−9815.
(11) Liu; Guyot-Sionnest, P. Mechanism of Silver(I)-Assisted Growth of Gold Nanorods and Bipyramids. *J. Phys. Chem. B* **2005**, *109*, 22192−22200.
(12) Hubert, F.; Testard, F.; Thill, A.; Kong, Q.; Tache, O.; Spalla, O. Growth and Overgrowth of Concentrated Gold Nanorods: Time Resolved SAXS and XANES. *Cryst. Growth Des.* **2012**, *12*, 1548−1555.
(13) Liu, Y.; Mills, E. N.; Composto, R. J. Tuning optical properties of gold nanorods in polymer films through thermal reshaping. *J. Mater. Chem.* **2009**, *19*, 2704−2709.
(14) Deshmukh, R. D.; Liu, Y.; Composto, R. J. Two-dimensional confinement of nanorods in block copolymer domains. *Nano Lett.* **2007**, *7*, 3662−3668.
(15) Meena, S. K.; Sulpizi, M. Understanding the Microscopic Origin of Gold Nanoparticle Anisotropic Growth from Molecular Dynamics Simulations. *Langmuir* **2013**, *29*, 14954−14961.
(16) Jana, N. R.; Gearheart, L.; Murphy, C. J. Evidence for seed-mediated nucleation in the chemical reduction of gold salts to gold nanoparticles. *Chem. Mater.* **2001**, *13*, 2313−2322.
(17) Ward, C. J.; Tronndorf, R.; Eustes, A. S.; Auad, M. L.; Davis, E. W. Seed-Mediated Growth of Gold Nanorods: Limits of Length to Diameter Ratio Control. *J. Nanomater.* **2014**, *2014*, 765618−765625.
(18) Sau, T. K.; Murphy, C. J. Seeded high yield synthesis of short Au nanorods in aqueous solution. *Langmuir* **2004**, *20*, 6414−6420.
(19) Lohse, S. E.; Eller, J. R.; Sivapalan, S. T.; Plews, M. R.; Murphy, C. J. A Simple Millifluidic Benchtop Reactor System for the High-Throughput Synthesis and Functionalization of Gold Nanoparticles with Different Sizes and Shapes. *ACS Nano* **2013**, *7*, 4135−4150.
(20) Jana, N. R. Gram-Scale Synthesis of Soluble, Near-Monodisperse Gold Nanorods and Other Anisotropic Nanoparticles. *Small* **2005**, *1*, 875−882.
(21) Ye, X. C.; Jin, L. H.; Caglayan, H.; Chen, J.; Xing, G. Z.; Zheng, C.; Doan-Nguyen, V.; Kang, Y. J.; Engheta, N.; Kagan, C. R.; Murray, C. B. Improved Size-Tunable Synthesis of Monodisperse Gold Nanorods through the Use of Aromatic Additives. *ACS Nano* **2012**, *6*, 2804−2817.
(22) Ye, X. C.; Zheng, C.; Chen, J.; Gao, Y. Z.; Murray, C. B. Using Binary Surfactant Mixtures To Simultaneously Improve the Dimensional Tunability and Monodispersity in the Seeded Growth of Gold Nanorods. *Nano Lett.* **2013**, *13*, 765−771.
(23) Ye, X.; Gao, Y.; Chen, J.; Reifsnyder, D. C.; Zheng, C.; Murray, C. B. Seeded Growth of Monodisperse Gold Nanorods Using Bromide-Free Surfactant Mixtures. *Nano Lett.* **2013**, *13*, 2163−2171.
(24) Wadams, R. C.; Fabris, L.; Vaia, R. A.; Park, K. Time-Dependent Susceptibility of the Growth of Gold Nanorods to the Addition of a Cosurfactant. *Chem. Mater.* **2013**, *25*, 4772−4780.
(25) Smith, D. K.; Korgel, B. A. The importance of the CTAB surfactant on the colloidal seed-mediated synthesis of gold nanorods. *Langmuir* **2008**, *24*, 644−649.
(26) Smith, D. K.; Miller, N. R.; Korgel, B. A. Iodide in CTAB Prevents Gold Nanorod Formation. *Langmuir* **2009**, *25*, 9518−9524.
(27) Park, H. J.; Ah, C. S.; Kim, W.-J.; Choi, I. S.; Lee, K.-P.; Yun, W. S. Temperature-induced control of aspect ratio of gold nanorods. *J. Vac. Sci. Technol., A* **2006**, *24*, 1323−1326.
(28) Kim, B. H.; Hackett, M. J.; Park, J.; Hyeon, T. Synthesis, Characterization, and Application of Ultrasmall Nanoparticles. *Chem. Mater.* **2014**, *26*, 59−71.
(29) Gai, P. L.; Harmer, M. A. Surface atomic defect structures and growth of gold nanorods. *Nano Lett.* **2002**, *2*, 771−774.
(30) Wei, Z. Q.; Zamborini, F. P. Directly monitoring the growth of gold nanoparticle seeds into gold nanorods. *Langmuir* **2004**, *20*, 11301−11304.
(31) Johnson, C. J.; Dujardin, E.; Davis, S. A.; Murphy, C. J.; Mann, S. Growth and form of gold nanorods prepared by seed-mediated, surfactant-directed synthesis. *J. Mater. Chem.* **2002**, *12*, 1765−1770.
(32) Jiang, X. C.; Pileni, M. P. Gold nanorods: Influence of various parameters as seeds, solvent, surfactant on shape control. *Colloids Surf., A* **2007**, *295*, 228−232.
(33) Park, K.; Drummy, L. F.; Wadams, R. C.; Koerner, H.; Nepal, D.; Fabris, L.; Vaia, R. A. Growth Mechanism of Gold Nanorods. *Chem. Mater.* **2013**, *25*, 555−563.
(34) Rayavarapu, R. G.; Ungureanu, C.; Krystek, P.; van Leeuwen, T. G.; Manohar, S. Iodide Impurities in Hexadecyltrimethyl ammonium Bromide (CTAB) Products: Lot-Lot Variations and Influence on Gold Nanorod Synthesis. *Langmuir* **2010**, *26*, 5050−5055.
(35) Pérez-Juste, J.; Liz-Marzán, L. M.; Carnie, S.; Chan, D. Y. C.; Mulvaney, P. Electric-Field-Directed Growth of Gold Nanorods in Aqueous Surfactant Solutions. *Adv. Funct. Mater.* **2004**, *14*, 571−579.
(36) Liu, J. C.; Duggan, J. N.; Morgan, J.; Roberts, C. B. Seed-mediated growth and manipulation of Au nanorods via size-controlled synthesis of Au seeds. *J. Nanopart. Res.* **2012**, *14*, 1289−1301.
(37) Gole, A.; Murphy, C. J. Seed-Mediated Synthesis of Gold Nanorods: Role of the Size and Nature of the Seed. *Chem. Mater.* **2004**, *16*, 3633−3640.
(38) Koerner, H.; MacCuspie, R. I.; Park, K.; Vaia, R. A. In Situ UV/Vis, SAXS, and TEM Study of Single-Phase Gold Nanoparticle Growth. *Chem. Mater.* **2012**, *24*, 981−995.
(39) Wagner, J.; Köhler, J. M. Continuous Synthesis of Gold Nanoparticles in a Microreactor. *Nano Lett.* **2005**, *5*, 685−691.
(40) Boleininger, J.; Kurz, A.; Reuss, V.; Soennichsen, C. Microfluidic continuous flow synthesis of rod-shaped gold and silver nanocrystals. *Phys. Chem. Chem. Phys.* **2006**, *8*, 3824−3827.
(41) Chan, E. M.; Alivisatos, A. P.; Mathies, R. A. High-temperature microfluidic synthesis of CdSe nanocrystals in nanoliter droplets. *J. Am. Chem. Soc.* **2005**, *127*, 13854−13861.
(42) Chan, E. M.; Mathies, R. A.; Alivisatos, A. P. Size-Controlled Growth of CdSe Nanocrystals in Microfluidic Reactors. *Nano Lett.* **2003**, *3*, 199−201.
(43) Elvira, K. S.; i Solvas, X. C.; Wootton, R. C. R.; deMello, A. J. The past, present and potential for microfluidic reactor technology in chemical synthesis. *Nat. Chem.* **2013**, *5*, 905−915.
(44) Nikoobakht, B.; El-Sayed, M. A. Preparation and growth mechanism of gold nanorods (NRs) using seed-mediated growth method. *Chem. Mater.* **2003**, *15*, 1957−1962.
(45) Philip, R.; Chantharasupawong, P.; Qian, H.; Jin, R.; Thomas, J. Evolution of Nonlinear Optical Properties: From Gold Atomic Clusters to Plasmonic Nanocrystals. *Nano Lett.* **2012**, *12*, 4661−4667.
(46) Alvarez, M. M.; Khoury, J. T.; Schaaff, T. G.; Shafigullin, M. N.; Vezmar, I.; Whetten, R. L. Optical Absorption Spectra of Nanocrystal Gold Molecules. *J. Phys. Chem. B* **1997**, *101*, 3706−3712.
(47) Kryachko, E. S.; Remacle, F. The magic gold cluster Au20. *Int. J. Quantum Chem.* **2007**, *107*, 2922−2934.

DOI: 10.1021/acs.chemmater.5b02675
Chem. Mater. 2015, 27, 6442−6449

(48) Gubicza, J.; Lábár, J. L.; Quynh, L. M.; Nam, N. H.; Luong, N. H. Evolution of size and shape of gold nanoparticles during long-time aging. *Mater. Chem. Phys.* **2013**, *138*, 449−453.
(49) Bastús, N. G.; Comenge, J.; Puntes, V. c. Kinetically Controlled Seeded Growth Synthesis of Citrate-Stabilized Gold Nanoparticles of up to 200 nm: Size Focusing versus Ostwald Ripening. *Langmuir* **2011**, *27*, 11098−11105.
(50) Liu, Y.; Kathan, K.; Saad, W.; Prud'homme, R. K. Ostwald ripening of beta-carotene nanoparticles. *Phys. Rev. Lett.* **2007**, *98*, 036102−036106.
(51) Sugimoto, T. Preparation of Monodispersed Colloidal Particles. *Adv. Colloid Interface Sci.* **1987**, *28*, 65−108.
(52) Jang, E.; Lim, E. K.; Choi, J.; Park, J.; Huh, Y. J.; Suh, J. S.; Huh, Y. M.; Haam, S. Br-Assisted Ostwald Ripening of Au Nanoparticles under H2O2 Redox. *Cryst. Growth Des.* **2012**, *12*, 37−39.
(53) Nightingale, A. M.; Krishnadasan, S. H.; Berhanu, D.; Niu, X.; Drury, C.; McIntyre, R.; Valsami-Jones, E.; deMello, J. C. A stable droplet reactor for high temperature nanocrystal synthesis. *Lab Chip* **2011**, *11*, 1221−1227.
(54) Voorhees, P. W. The Theory of Ostwald Ripening. *J. Stat. Phys.* **1985**, *38*, 231−252.
(55) Snyder, V. A.; Alkemper, J.; Voorhees, P. W. The development of spatial correlations during Ostwald ripening: A test of theory. *Acta Mater.* **2000**, *48*, 2689−2701.
(56) Thessing, J.; Qian, J.; Chen, H.; Pradhan, N.; Peng, X. Interparticle influence on size/size distribution evolution of nanocrystals. *J. Am. Chem. Soc.* **2007**, *129*, 2736−2737.
(57) Kang, C. H.; Yoon, D. N. Coarsening of Cobalt Grains Dispersed in Liquid Copper Matrix. *Metall. Trans. A* **1981**, *12*, 65−69.
(58) Snyder, V. A.; Alkemper, J.; Voorhees, P. W. Transient Ostwald ripening and the disagreement between steady-state coarsening theory and experiment. *Acta Mater.* **2001**, *49*, 699−709.
(59) Yang, J. A.; Lohse, S. E.; Boulos, S. P.; Murphy, C. J. The Early Life of Gold Nanorods: Temporal Separation of Anisotropic and Isotropic Growth Modes. *J. Cluster Sci.* **2012**, *23*, 799−809.
(60) Lewis, L. J.; Jensen, P.; Barrat, J. L. Melting, freezing, and coalescence of gold nanoclusters. *Phys. Rev. B: Condens. Matter Mater. Phys.* **1997**, *56*, 2248−2257.
(61) Cleveland, C. L.; Luedtke, W. D.; Landman, U. Melting of gold clusters: Icosahedral precursors. *Phys. Rev. Lett.* **1998**, *81*, 2036−2039.
(62) Barnard, A. S.; Young, N. P.; Kirkland, A. I.; van Huis, M. A.; Xu, H. Nanogold: A Quantitative Phase Map. *ACS Nano* **2009**, *3*, 1431−1436.
(63) Koga, K.; Ikeshoji, T.; Sugawara, K. Size- and temperature-dependent structural transitions in gold nanoparticles. *Phys. Rev. Lett.* **2004**, *92*, 11507−11511.
(64) Mikami, Y.; Dhakshinamoorthy, A.; Alvaro, M.; Garcia, H. Catalytic activity of unsupported gold nanoparticles. *Catal. Sci. Technol.* **2013**, *3*, 58−69.
(65) Turner, M.; Golovko, V. B.; Vaughan, O. P. H.; Abdulkin, P.; Berenguer-Murcia, A.; Tikhov, M. S.; Johnson, B. F. G.; Lambert, R. M. Selective oxidation with dioxygen by gold nanoparticle catalysts derived from 55-atom clusters. *Nature* **2008**, *454*, 981−983.
(66) Corma, A.; Garcia, H. Supported gold nanoparticles as catalysts for organic reactions. *Chem. Soc. Rev.* **2008**, *37*, 2096−2126.

DOI: 10.1021/acs.chemmater.5b02675
Chem. Mater. 2015, 27, 6442−6449